Experimental Assessment of Antimony (Sb) in Pure Uranium for Immobilizing Fission Product Lanthanides

Weiqian Zhuo[a], Yi Xie[b], Michael T. Benson[b], Huali Wu[a], Robert D. Mariani[b], Jinsuo Zhang[a,*],

[a] Nuclear Engineering Program, Department of Mechanical Engineering
Virginia Polytechnic Institute and State University, Blacksburg, Virginia 24061, USA
[b] Idaho National Laboratory, P.O. Box 1625, MS 6188, Idaho Falls, ID 83415, USA
*Corresponding author, Email: zjinsuo5@vt.edu

Abstract

The use of fuel additives is one of the concepts to mitigate fuel cladding chemical interaction (FCCI) for metallic fuel because fission product lanthanides are expected to be immobilized by the additive. Antimony (Sb) has been found to be a good candidate in UZr fuel. The present study focuses on its mechanism for immobilization in pure uranium, U-4Sb alloy was fabricated to understand the Sb behavior, while U-4Sb-4Ce was fabricated to simulate the case when lanthanides are generated. Both of the as-cast and annealed samples were characterized by scanning electron microscope (SEM) and energy dispersive spectrometer (EDS). U-Sb precipitates are formed in U-4Sb alloy, while U-Sb and Ce-Sb were found in U-4Sb-4Ce alloy, thermal exposure does not change the Sb-precipitation morphologies or chemical composition. In addition, diffusion couple tests between those alloys and cladding materials (Fe or HT9) under 650 ℃ for 500 hours were performed and analyzed using SEM/EDS. Diffusion couple tests show the reaction between cladding and uranium, while no reaction between Sb-precipitations and cladding materials was found.

Keywords – Metal fuel; additive antimony; diffusion couple tests; SEM/EDS;

1. Introduction

Fuel cladding chemical interaction (FCCI) is a phenomenon that occurs at the interface between fuel and cladding, and it would result in a multi-phase region that places both the fuel and cladding at risk [1]. A major cause of FCCI in metallic fuels during irradiation is fission product lanthanides (Ln, e.g., Ce, Pr, and Nd)-cladding interaction due to Ln migration to the fuel periphery and the swelling fuel contacting with cladding [2]. Several concepts have been proposed in order to mitigate FCCI, the additive method is one of them and it has been studied in recent years [2]. Available studies on some selected additives include Pd [3] [4], Sn [5], Sb [6], Te [7], In [8, 9], Tl [9], Ga [9], and Sn/Sb mixtures [10]. Among those candidates, assessments on antimony (Sb) showed that it could be a promising additive. The assessments include out-of-pile UZr fuel-additive alloy test [6] [11] [12], lanthanide-additive compounds /cladding diffusion couple test [13] [14], and modeling using the Bozzolo-Ferrante-Smith (BFS) method [9]. Some demonstrated or potential advantages of adopting Sb as the additive could be summarized as the following: (1)

In U-10Zr fuel, Sb has the preference to bind lanthanide (e.g. Ce) over Zr [6]; (2) Sb-lanthanide compounds are thermodynamically stable and compatible with cladding [13] [14]; (3) Sb may have higher preference to bind lanthanides compared to other candidates such as Sn [10] or In, Tl, and Ga [9].

In U-Zr or U-Pu-Zr fuel, Zr redistribution is commonly observed in two major cases. One is due to the temperature gradient where Zr redistribution takes place inside the fuel along the ΔT [15]. The other is the Zr-rind formation at the fuel periphery most likely due to the impurities such as C, O, or N [16]. In U-Zr fuel, Zr redistribution in both cases will result in a region enriched in uranium. For example, fuels taken from Fast Flux Test Facility (FFTF) show an annular region that is depleted in zirconium and enriched in uranium, effectively caused by the migration of Zr to fuel center [17]. Consider the extreme case, it is possible to have a Zr-free area and only composite of pure U inside the UZr fuel. Regarding the second case, we could look at another example by out-of-pile diffusion couple test using UZr against Fe [18], Zr had migrated to the fuel periphery and formed a rind attached to Fe, exhibited a region enriched in uranium in the fuel side. In the event that Zr-rind is not intact [16], direct contact between U and cladding could take place.

Since Sb is also a fission product [19], the fission yield is small (1.30% per fission for U-238[*] [20]) but it will be more likely to generate in the pure U phase where there is no free Zr, especially if the reactor could reach higher burnup in the future. Focusing on Zr-free region, there are four possible ways the produced Sb would behave: (1) formed as free Sb that is dissolved into the fuel matrix and transport to cladding like other lanthanide fission products; (2) free Sb that is metal precipitate; (3) combined with U; (4) combine with other fission products. Free Sb is not desirable, because Sb would attack Fe [21, 22] to form lower melting eutectic phase (based on the phase diagram [23]). Therefore, Zr-free alloy is proposed in this work to gain a better understanding of Sb mechanism in a pure U region of UZr fuel, either inside the fuel or at the fuel periphery.

In addition, there are two other reasons for focusing on Zr-free alloys in the study. First, from the experimental point of view, when evaluating the compatibility between cladding materials and UZr fuel using diffusion couple method, it was reported that the major interactions are between U and cladding, however, Zr-rind might form [18][24][25] during the tests, preventing cladding materials such as Fe from diffusing deep into the U-Zr side of the couple [1]. This problem can be easily avoided in this work. Second, the feasibility and possibility of Zr-free alloys have been proposed and studied recently in BN-type fast reactor [26][27], this study, therefore, can also provide a pioneering view for such applications.

The investigation in this paper is a continuation of previous work [6] using Sb as a minor additive to control FCCI, but emphasizing in Zr-free zone and considered Sb as a fission product or

[*] This is the cumulative fission yield considered the fast fission yield and 14-MeV fission yield of Sb-122, Sb-124, and Sb-125 for U-238

additive. The previous work focused on U-10Zr (a typical fuel composition for sodium cool fast reactor, weight percent), the U-10Zr-4Sb and U-10Zr-4Sb-4Ce alloys were investigated [6]. For comparison, two Zr-free alloys were studied in the present work, i.e., U-4Sb and U-4Sb-4Ce. Thus, a separate effect evaluation can be performed to isolate the behavior in U-10Zr fuel. With this motivation, U-4Sb (wt%) alloy was fabricated. To simulate the Ln generation, Ce is used to represent Ln and therefore, U-4Sb-4Ce (wt%) alloy was fabricated accordingly.

The evaluation includes three parts. Firstly, as-cast samples were analyzed to obtain benchmark information. Secondly, the samples were heated to identify if the microstructure including the precipitate chemical composition would change upon heat treatment. To understand the stability of Sb compounds formed in alloy and the FCCIs, the third step is to perform diffusion couple tests to assess the compatibility between those alloys and Fe-based cladding materials. The cladding materials used in this work are Fe and HT9. All the samples in three tests were independent to each other. Details about the materials and experiments will be described in section 2.

2. Materials and experiment

The U-4Sb and U-4Sb-4Ce alloys were fabricated by arc melting. All materials, except U, were obtained from Alfa Aesar and used as received. Ce was obtained as a rod, packaged in mylar under argon. U was cleaned by submersion in nitric acid, followed by a water wash, then an ethanol wash. All casting operations were carried out in an arc-melter within an argon atmosphere glovebox with high purity argon as a cover gas. To prepare the U-4Sb alloys, the appropriate amount of Sb and U were arc melted together. To prepare the alloys with Ce, the appropriate amount of Ce was added to a pre-alloy button of U-4Sb alloy. After each additive step, the resulting cast button was flipped and re-melted three times to ensure homogeneity. The buttons were cast into 5 mm diameter rods then sectioned into 2 mm thick pins for all the experiments.

The thermal exposure tests were performed in furnace (Thermo Scientific Thermolyne FB1415M) which was calibrated between 550 ℃ ~750 ℃ within the error of ± 0.2%. Furnace was placed in a high purity argon-filled glovebox (Inert PL-HE-4GB-2500). For diffusion couple tests, each USb alloy (U-4Sb or U-4Sb-4Ce) sample was coupled with Fe on one side and HT9 on the other side as shown in Figure 1. Fe foil (99.994%) was purchase from Alfa Aesar. HT9 was provided by Los Alamos National Laboratory, the elemental composition is shown in Table 1, and more details can be found in Ref [28].

Table 1. Composition of the HT9.

Element	wt. %	Element	wt. %	Element	wt. %
O	0.016	P	0.007	Si	0.39-0.40
N	0.031	Co	0.009	Cr	12.1

C	0.171	Cu	0.018	Mo	0.92
S	0.004	Ti	0.002	Ni	0.60
V	0.31	Fe	84.2	Al	0.006
W	0.58	Mn	0.59	-	-

Before assembling the couple samples, the surfaces were ground with SiC grinding paper followed by polishing with polycrystalline diamond suspensions to 1 μm. The samples were cleaned by deionized water and dried. Then the samples were coupled together, wrapped in Ta foil and clamped in Kovar fixture. The heat treatment conditions for thermal exposure tests and the diffusion couple tests were set to 650°C for 500 hours.

After heat-treatment, the samples were quenched in Si-based oil (in glovebox) to preserve the high-temperature phase equilibrium. The samples were mounted in epoxy (for diffusion couple tests, the samples were cut perpendicularly to reveal the interface after mounting), then the surfaces were ground with SiC grinding paper followed by polishing with polycrystalline diamond suspensions to 1 μm in air. A coating of Au/Pd (60/40 in wt. %) was applied, and the thickness of the coating was around 4.5 nm. The SEM (model:FEI Quanta 600 FEG) is equipped with a Bruker energy dispersive spectrometer (EDS). The SEM was operated at an accelerating voltage of 20 kV and spot size 5. EDS data was collected by ESPRIT 1.9, the spectra were collected up to 10 keV. L-α and K-α of Cu (standard) was used for energy calibration. In this study, the point analysis, line scan and mapping were applied. The point analysis and line scan were used for concentration measurement, while mapping was used to determine the elemental distribution. For concentration measurement, the net counts above background were used for deconvolution and quantification. The deconvolution and quantification method were serials fit and P/B ZAF (standardless). For the maps, raw count signals were displayed. U M-series, Sb L-series, Ce L-series, Fe K-series, Cr K-series were used for point analysis. U-Mα, Sb-Lα, Ce-Lα, Fe-Kα, Cr-Kα were used for the line scan and map analysis.

To provide a theoretical baseline of the accuracy of EDS, an estimation was done for spatial resolution and interactive volume of the electron beam in the uranium metal (bulk material in fuel alloy). An approximate spatial resolution can be calculated from the expression of Anderson and Hasler that is recommended in Ref [29]: $R_x(\mu m) = 0.064(E_0^{1.68} - E_c^{1.68})/\rho$, where E_0 is the electron accelerating voltage of 20 keV, Ec is the excitation voltage for U-Mα line at 3.171 keV (the strongest peak), ρ is the uranium density which is 19.10 g/cm^3. Hence, the theoretical spatial resolution in uranium is 0.49 μm. To obtain the interaction volume further, it is assumed that the electron beam would interact with the material in an idea spherical volume. The radius of the spherical volume is half of the penetration depth, and the penetration depth is considered to be equivalent to the spatial resolution. Accordingly, the theoretical interaction volume is calculated to be 0.062 μm^3.

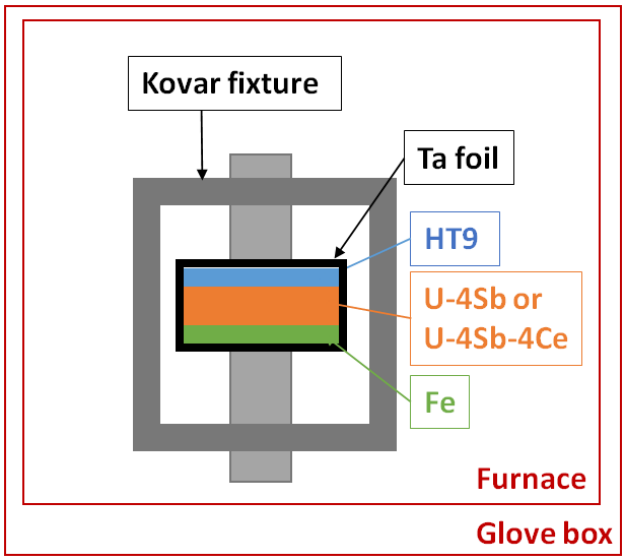

Figure 1. Schematic diagram of diffusion couple test

3. Results

In section 3.1, as-cast samples as well as the heat-exposure samples were characterized. It mainly focuses on the microstructure formed in U-4Sb alloy, and estimate the effects on the Sb performance with Ce when it is presented. In section 3.2, the diffusion behaviors between alloys and claddings were analyzed. All the image shown in this section were taken under backscattered electron (BSE) mode unless specified otherwise.

3.1 SEM/EDS characterization

3.1.1 As-cast samples

3.1.1.1 U-4Sb

The overview morphology of the as-cast sample under BSE is shown in Figure 2 (a). The bright region is matrix and the dark regions are precipitates. The typical structures for the precipitates observed are long strips and irregular polygon spots. The strips are uniformly distributed in the fuel and commonly 30 – 50 μm long, some of them are overlapped to form even longer strips. Indicated by EDS point data, there are three phases found: the bright matrix is U, the black and grey precipitates are two U-Sb phases with different compositions. Typical morphologies and the corresponding point data are shown in Figure 2 (b-c) and Table 2. Selected EDS point spectra together with a spectrum from standard uranium sample (high purity uranium metal, provided by INL) are shown in Figure 2 (d).

In the quantified result, the matrix (point 1 and point 2) contains small fraction of Sb. This fraction could be resulted from M_V edge peak of U, i.e., the U-M_V edge (3.552 keV) contributes to Sb-$L\alpha_1$

peak (3.604 keV) [30]. This is verified by checking the standard uranium sample using the identical configuration. As shown in Figure 2 (d), the main peaks of point 1 are well matched with that of standard uranium. The solubility of Sb in α-U was reported to be approximately 0.02 at. % at 620 °C [31]. With the limitation of the EDS, it is not expected to differentiate or detect Sb solubility in U.

For the U-Sb precipitates, in this study, they have two typical compositions under EDS, the dark precipitates are mainly composed of ~57 at% U (point 3 – 5 in Figure 2 b, point 9 – 11 in Figure 2 c), and the gray precipitates that have higher uranium concentration varied from 62~ 65 at% (point 6 and 7 in Figure 2 b, point 12 – 14 in Figure 2 c). The spectra of point 3 and point 6 are shown in Figure 2 (d). The two main uranium peaks are from U-Mα and U-Mβ lines, and the two main antimony peaks are from Sb-Lα_1 and Sb-Lβ_1 lines. The antimony intensities from both spectra are close, while the uranium intensity of point 3 is higher than that of point 6, thus resulting a higher uranium content. In terms of the phase quantification using EDS, there are two points need to be noticed here. First, it is noticed that the precipitates may be protruded from the surface (verified by secondary electrons images), and it is known that the uneven surface would affect the quantification results [32]. Second, the point quantification results on precipitation could be affected by the matrix. Due to the absorption of X-ray, across uranium signal from the matrix could have contributed to the U-Sb phase and perturb the fraction. Considered these two statements, it is believed that: (1) the dark precipitates could be U_4Sb_3 or U_5Sb_4 based on the available studies [31] [33] [34], the compositions between those two phases are too closed to be differentiated under EDS; (2) the grey phases could be a new phase but it is not conclusive in this study.

In summary, Sb is mainly found in the form of U-Sb precipitates, limited by the EDS resolution, the exact phase cannot be identified. There are no free or significant level of Sb found. In UZrSb alloy, Sb is found to combine with Zr (Zr_2Sb was identified) [6], while U-Sb phase was not found, this implies Sb has higher affinity to Zr over U. This suggests Sb would combine with Zr in U-10Zr alloy, and as the pure uranium region formed during operation, Sb would form precipitates with U.

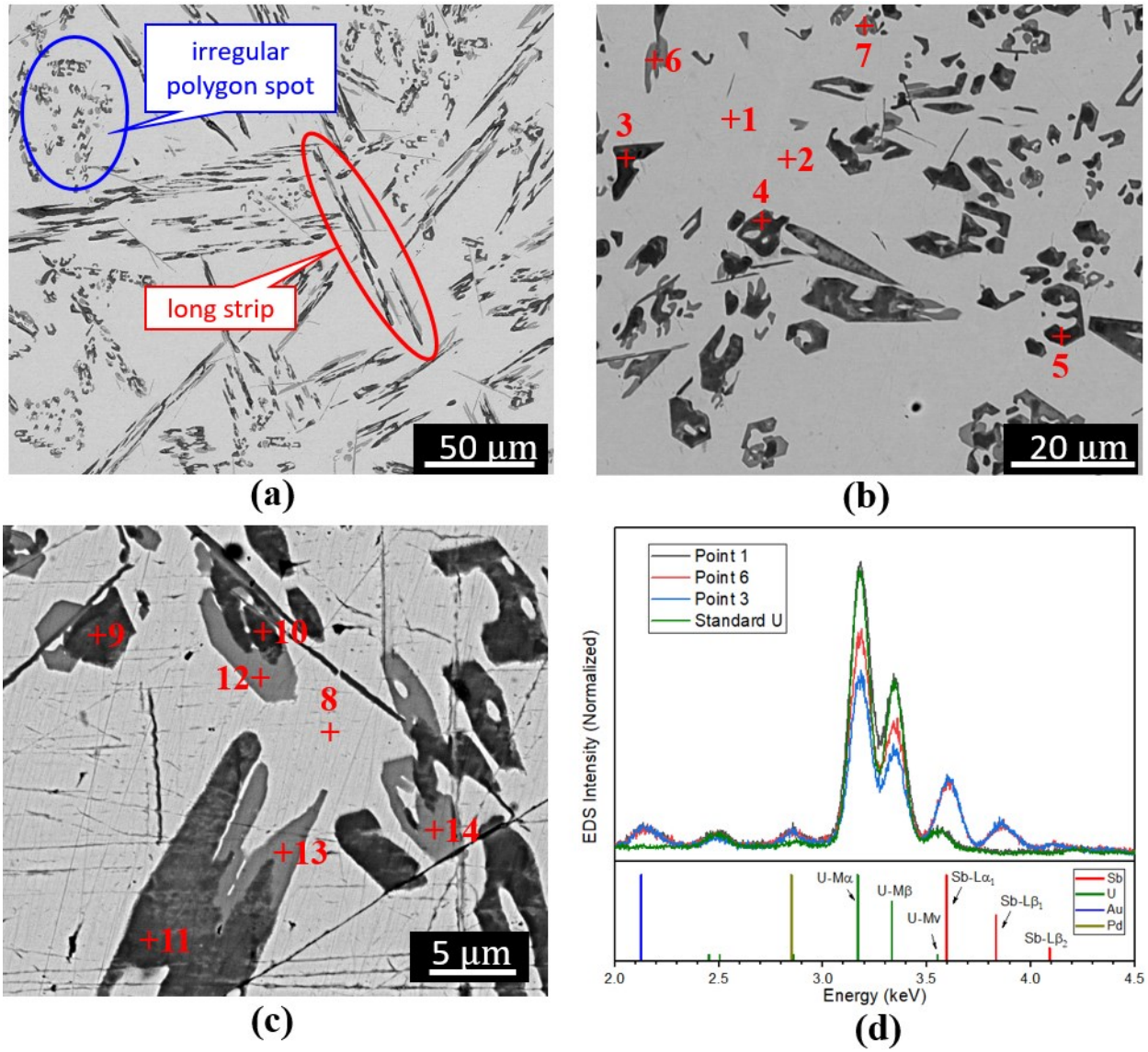

Figure 2. As-cast U-4Sb alloy at multi scales: (a) magnification of 1000×, (b) magnification of 3000×, and (c) magnification of 8000×. The corresponding point data is listed in Table 2. (d) Selected EDS point spectra together with a spectrum from standard uranium. Au and Pd are presented in point 1, 6, and 3 because they were the coating materials, but note that the standard uranium was not coated when performing the analysis.

Table 2. EDS data for points in Figure 2 (b) and (c) (at. %)

	U	Sb	Phase*
1	97.2	2.8	U
2	97.3	2.7	U
3	57.0	43.0	U_4Sb_3 or U_5Sb_4
4	56.9	43.1	U_4Sb_3 or U_5Sb_4
5	57.3	42.7	U_4Sb_3 or U_5Sb_4

6	62.6	37.4	-
7	65.4	34.6	-
8	98.9	1.1	U
9	57.4	42.6	U_4Sb_3 or U_5Sb_4
10	58.4	41.6	U_4Sb_3 or U_5Sb_4
11	57.5	42.5	U_4Sb_3 or U_5Sb_4
12	63.9	36.1	-
13	64.2	35.8	-
14	64.2	35.8	-

* Phase suggested by EDS point data, see text for further explanation.

3.1.1.2 U-4Sb-4Ce

For U-4Sb-4Ce alloy, the overview morphology of the as-cast sample is shown in Figure 3 (a), it has the same magnification to Figure 2(a), but the microstructure of the precipitates changed as Ce is presented. The grey region is U-Sb and the dark small spots are Ce-Sb precipitates. Compared to U-4Sb alloy, the U-Sb stripes are found to be shorter in U-4Sb-4Ce alloy. When fabricating the U-4Sb-4Ce alloy, Ce was added into the pre-made U-4Sb alloy. Therefore, the shorter U-Sb stripes in U-4Sb-4Ce alloy indicates that the decomposition takes place for U-Sb precipitates with the addition of Ce.

In Figure 3 (b), it is found that most of the Ce-Sb precipitations are in the size of several micrometers, some precipitations are in the size of around 10 μm. The EDS point data on the precipitate (point 5 and point 6 in Figure 3b) shows it contains ~ 49 at. % Sb and ~ 42 at. % Ce. It suggests that the phase is CeSb compound according to the phase diagram [35]. In Ce-Sb system, the enthalpy of formation for CeSb is the most negative compared to other compounds (Ce_2Sb, Ce_4Sb_3, and $CeSb_2$) [13]. This indicates CeSb is the most stable phase, and the formation of CeSb is most likely. In U-Zr-Sb-Ce alloy [2], some very large (up to ~100 μm in length) Ce_2Sb and Ce_3Sb_4 were identified. In this case, however, Ce-Sb precipitates at much smaller size were found. The reason is not clear, but it is well known that the formation of the phases could be affected by the casting process [7] as well as the fuel composition.

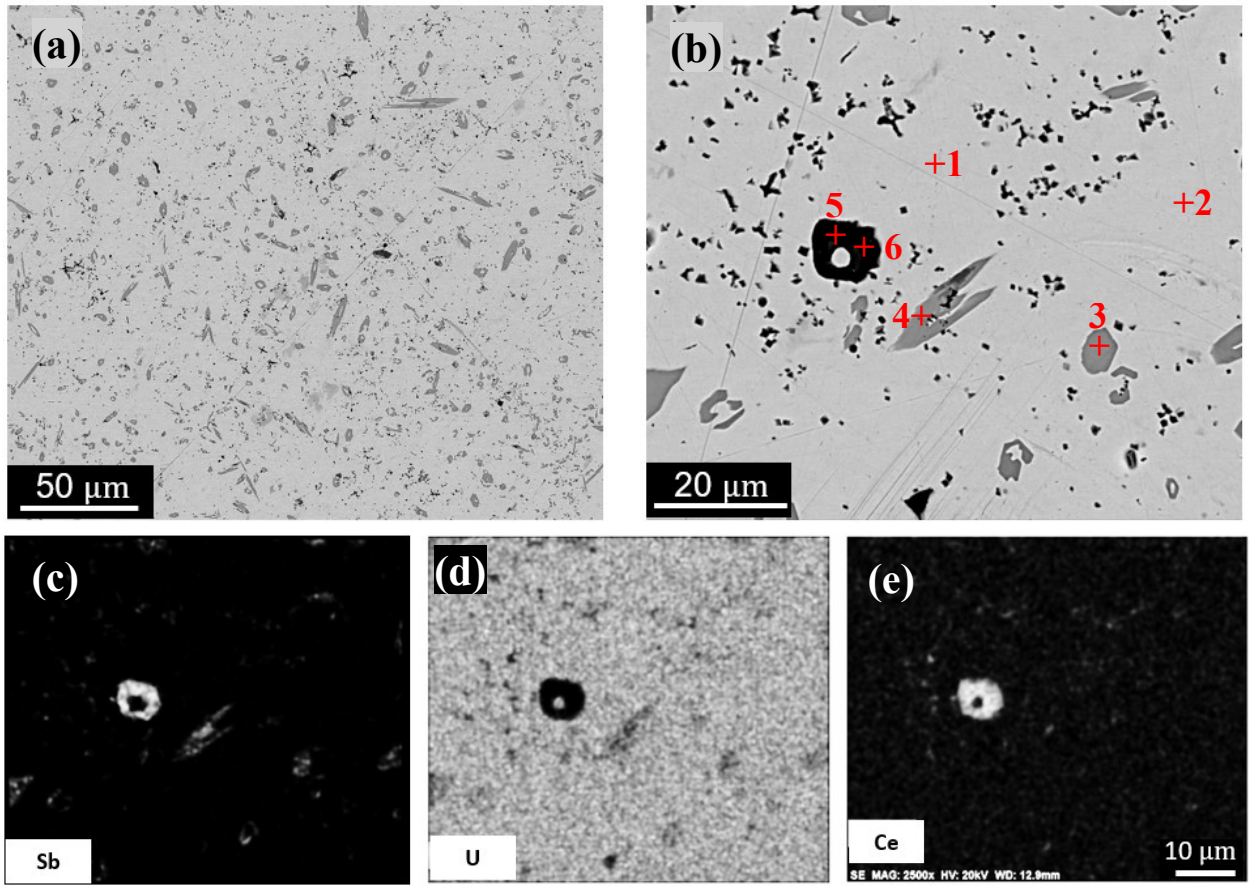

Figure 3. As-cast U-4Sb-4Ce alloy at (a) magnification of 1000×, (b) magnification of 3000×. (c) – (d) are elemental maps of Sb, U, and Ce for (b).

Table 3. EDS data for points in Figure 7(at. %)

	U	Sb	Ce	Phase*
1	97.4	2.6	0.0	U
2	98.3	1.7	0.0	U
3	63.5	36.5	0.0	-
4	65.3	34.4	0.3	-
5	9.0	48.5	42.5	CeSb
6	8.9	49.0	42.1	CeSb

* Phase suggested by EDS point data, see text for further explanation.

3.1.2 Heat-exposure samples

The U-4Sb and U-4Sb-4Ce alloys also heated under 650 °C for 500 hours. The overall morphologies of U-4Sb and U-4Sb-4Ce alloy are presented in Figure 4 (a) and Figure 4 (c) respectively. Visually, the morphologies are similar to that of the as-cast sample (Figure 2a and Figure 3b). The EDS point analysis is performed on Figure 4 (b) for U-4Sb alloy and on Figure 4 (d) for U-4Sb-4Ce alloy, and the corresponding data is listed in Table 4. The point data indicates the phase composition of the annealed alloy is consistent with that of as-cast sample. The

morphological and the compositional analysis shows that the Sb-precipitates are stable under the given heat treatment condition.

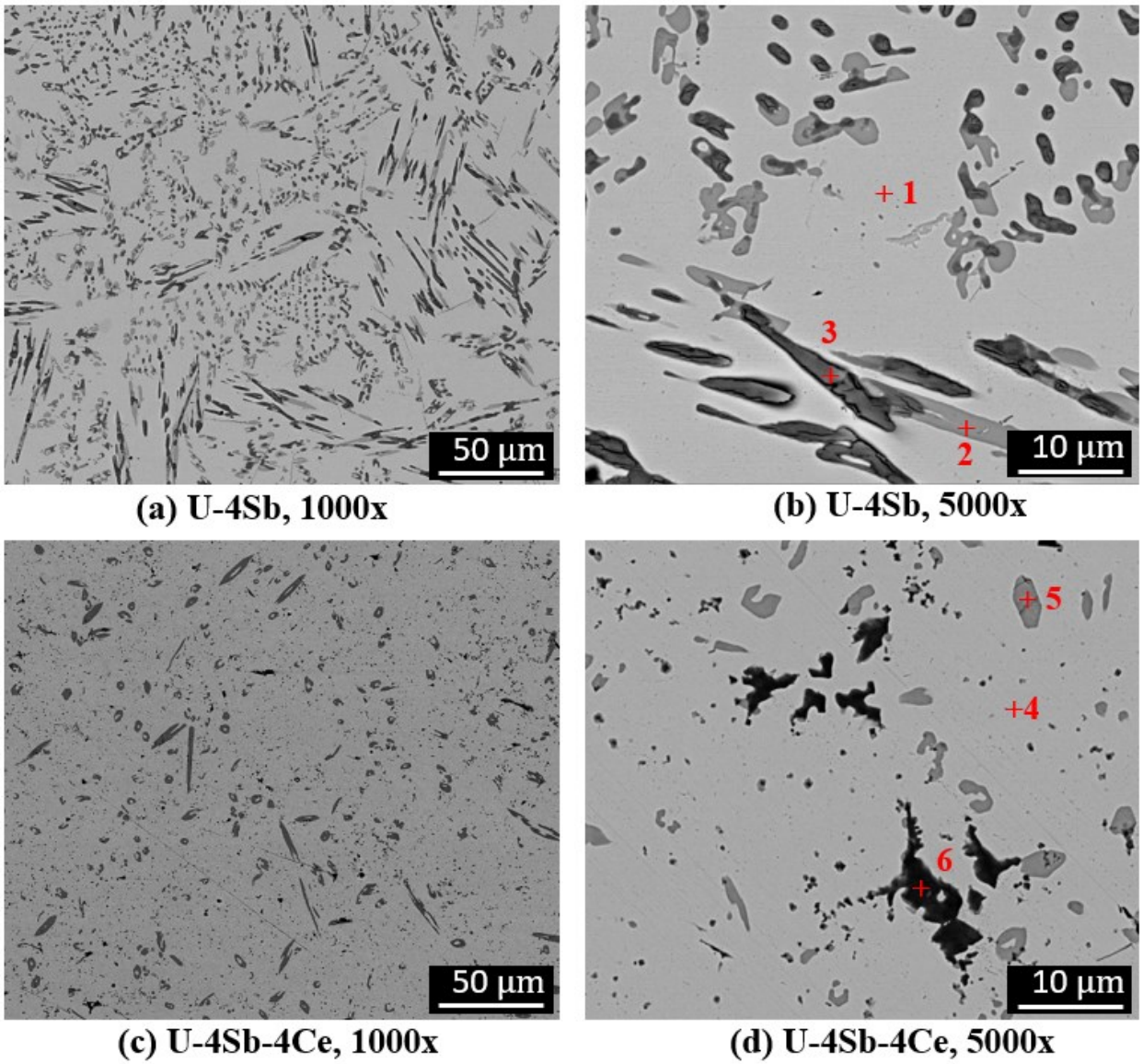

Figure 4. Results for the heat exposure test samples. The EDS point data is listed in Table 4.

Table 4. EDS data for points in Figure 4 (at. %)

Point	U	Sb	Ce	Phase*
(b)				
1	97.9	2.1	-	U
2	63.9	36.1	-	-
3	57.4	42.6	-	U_4Sb_3 or U_5Sb_4
(d)				
4	98.3	1.7	0.0	U

5	64.1	35.0	0.0	-
6	7.9	47.7	44.4	CeSb

* Phase suggested by EDS point data.

3.1.3 Sb-precipitate size distribution analysis

Since the microstructure is determined by the Sb-precipitate size, a quantified size analysis was carried out. The analysis was based on Figure 2a (as-cast U-4Sb), Figure 3a (as-cast U-4Sb-4Ce), Figure 4a (heat-exposure U-4Sb) and Figure 4c (heat-exposure U-4Sb-4Ce). There are two steps to perform the analysis. Step one, an BSE image was analyzed by ImageJ [36] to obtain and the size histogram of Sb-precipitates. Step two, the histogram data was normalized to obtain the size distribution. In step one, the precipitate size threshold was set to 1 μm^2 in ImageJ. The 1 μm^2 threshold was chosen in accordance to the limitation of the EDS resolution. Below the resolution, the feature of the region was not differentiable.

The analyzed results are plotted in Figure 5. It is found that the precipitate size (cross-section) is varied from 1 to 300 μm^2, and most of the precipitate are smaller than 20 μm^2. The major difference between U-4Sb and U-4Sb-Ce alloy is the fraction of the size between 1 to 2 μm^2. It is around 20% for U-4Sb, while this fraction is doubled for U-4Sb-4Ce. By comparing the data between as-cast sample and heat-exposure sample, the change is not significant. This will support the argument that the Sb-precipitates are stable upon heat exposure.

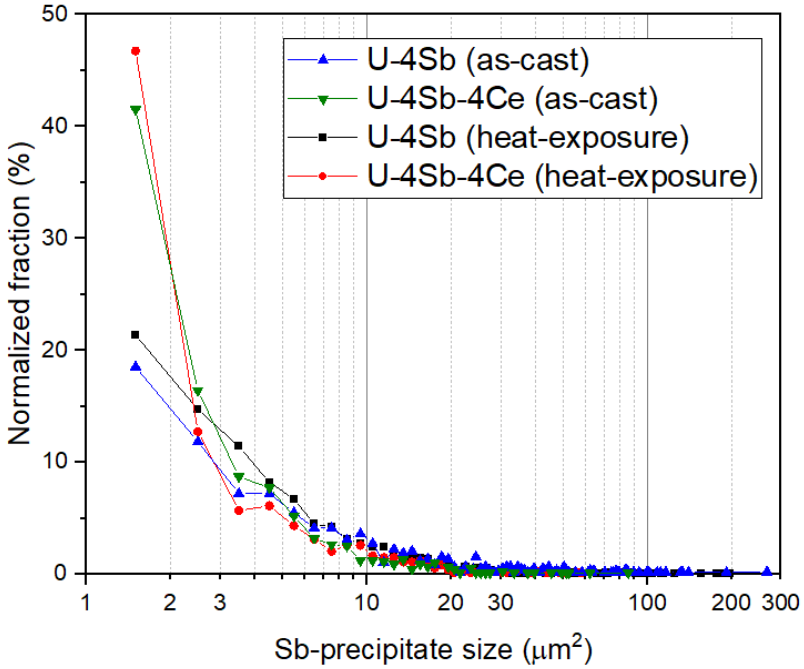

Figure 5. The Sb-precipitates distribution for as-cast samples and heat-exposure samples.

3.2 Diffusion couple tests

The diffusion behavior between the alloy and Fe-based cladding materials will be discussed in this section. In general, it is found that the inter-diffusion layers between Fe and USb alloy (U-4Sb or U-4Sb-4Ce) are UFe_2 and U_6Fe. UFe_2 layer is formed at Fe side, and U_6Fe layer is formed between UFe_2 and unreacted USb alloy matrix. For HT9 and USb alloy, inter-diffusion layers were found to be $U(Fe,Cr)_2$ at HT9 side and U_6Fe at USb alloy side. Typical element compositions and thicknesses for the reaction layer are summarized in Table 5. More details associated with those layers will be described in the following sections. For better discussion, three layers (i.e., layer-I, II, and III) are marked in the interfacial images. Layer-I refers to cladding material, Fe or HT9. Layer-II is UFe_2 or $U(Fe,Cr)_2$, such phases are so-called laves phase [37] [38] [39]. Layer-III is U_6Fe which contains U_4Sb_3 precipitates or Ce-Sb precipitates.

Table 5. Representative element compositions and thickness for the reaction layer

Cladding material	Reaction layer	Composition (at. %)				Thickness (μm)
		U	Sb	Fe	Cr	
Fe	UFe_2	32.0	0.8	67.2	-	3~10
	U_6Fe	82.7	2.0	15.3	-	180~210
HT9	$U(Fe,Cr)_2$	34.3	0.4	49.7	15.6	10~20
	U_6Fe	83.3	2.2	14.4	0.1	150~160

Note: the composition data is averaged from at least 5 different points that randomly distributed at three different areas on the coupled interface; the thickness is taken from at least 3 different locations at least 100 microns apart.

3.2.1 U-4Sb/cladding

The inter-diffusion layers between Fe and U-4Sb alloy are UFe_2 and U_6Fe. In the available studies of U/Fe diffusion couple tests, as reported in Ref [40] and [41], the diffusion layers of UFe_2 and U_6Fe have been confirmed. For U-4Sb alloy, as we discussed in section 3.1, Sb mainly existed as U-Sb precipitates, and the matrix is U. The interaction between Fe and U in our results are comparable and consistent with U/Fe system. An overview BSE image of U-4Sb/Fe interface (magnification 1000×) and a line scan analysis are shown in Figure 6. The regions from left to right are Fe, UFe_2, U_6Fe and unaffected U-matrix. The thickness of the UFe_2 and U_6Fe region is around 10 μm and 190 μm, respectively. Visually, the morphology, size, and density of precipitates in the U_6Fe region are similar to that in unaffected matrix.

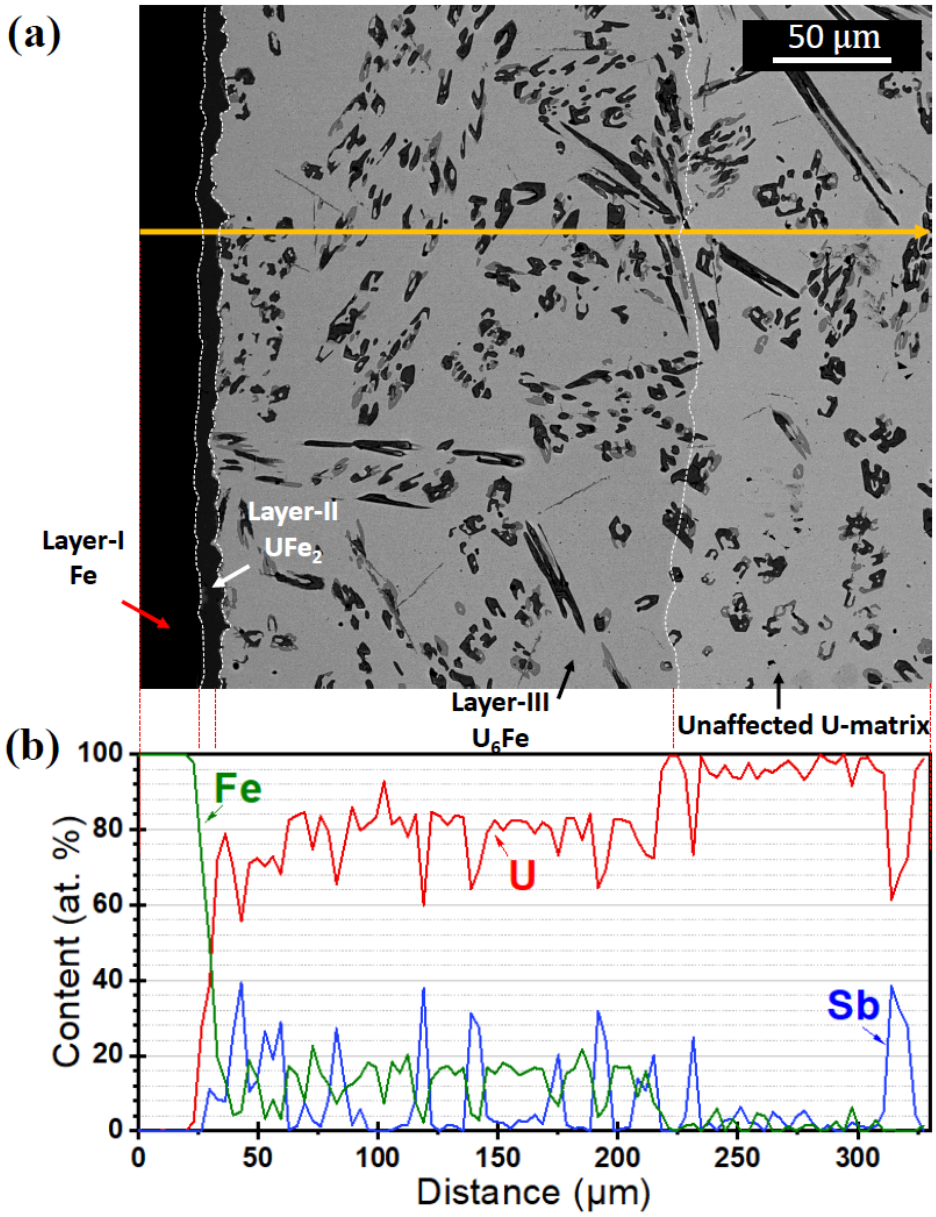

Figure 6. (a) An overview BSE image of U-4Sb/Fe interface, the reaction layers are marked by dash line; (b) elemental distribution for the scan line.

An image with magnification of 5000× at the U-4Sb/Fe interface is shown in Figure 7 (a). The presented phases can be identified by the point data (Table 6), line scan data (Figure 7b), and elemental maps (Figure 7 c to e). In layer-III, the bright zone is U_6Fe that contains U-Sb precipitates. According to the line scan data, it is noticed that the Fe fraction significantly drop when the line passes U-Sb precipitates (x = 24 – 30 µm and x = 52 – 55 µm). The point analysis was performed on U-Sb precipitates, and the average composition is 61.7% U, 37.3% Sb and 1.0% Fe (atom percent). The Fe fraction can be treated as noise due to UFe_6 matrix. Based on the line

and point data, it is suggested that Fe does not diffuse into U-Sb precipitates. Layer-II is UFe_2, it appears to "separate" the U-Sb precipitates with Fe. From the map in Figure 7 (e), Sb seems to be "cut-off" at the interface of layer-II (UFe_2). If the Sb-precipitates is a "marker", then this suggests the UFe_2 is formed by outward diffusion of uranium, while UFe_6 is formed by inward diffusion of Fe into the fuel alloy. According to the map, no binary phase between Fe and Sb was found, neither the ternary phase between Fe, U, and Sb was found.

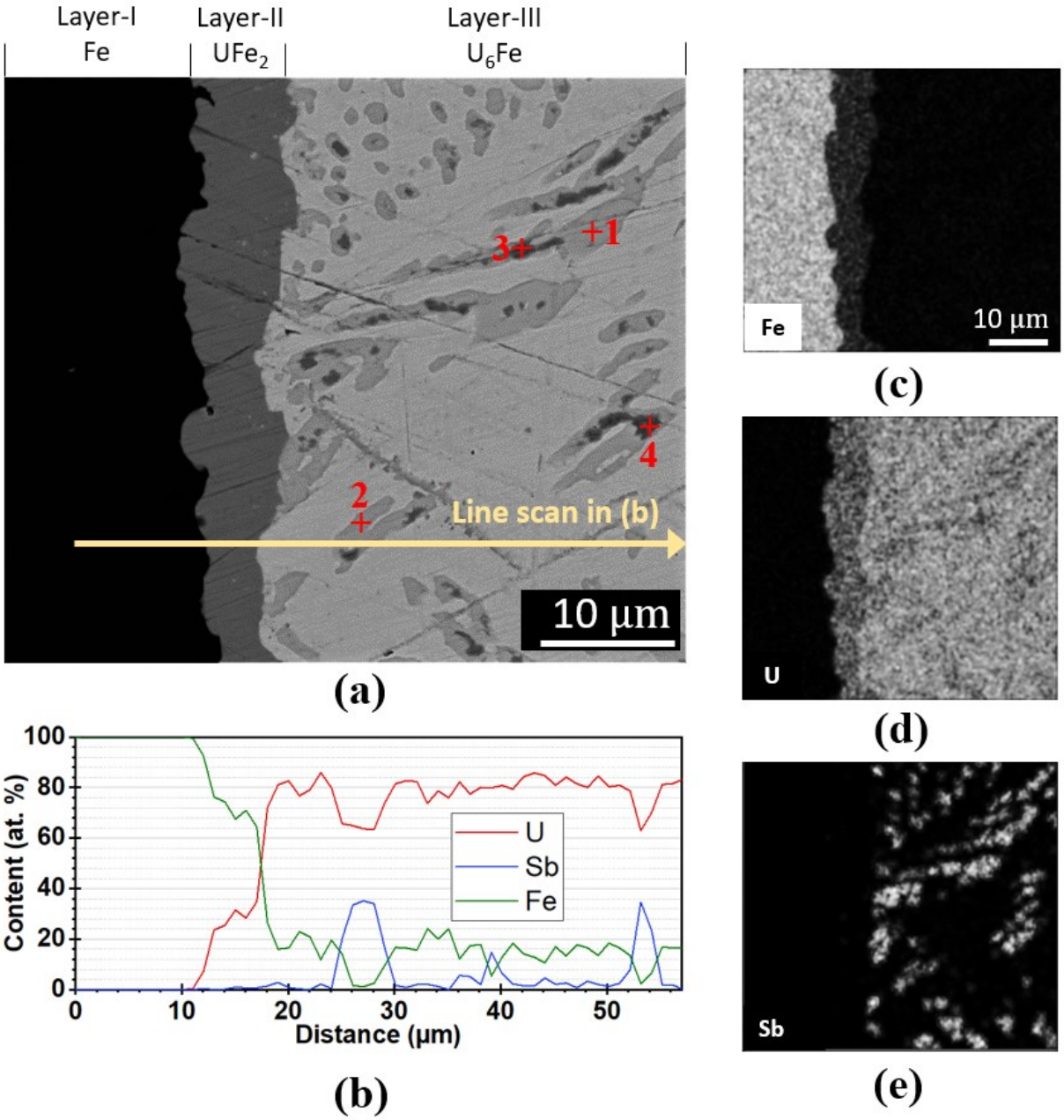

Figure 7. (a) U-4Sb/Fe interface, (b) elemental distribution corresponding to the scan line, (c)~(e) are elemental maps of Fe, U, Sb for (a).

Table 6. EDS data for points in Figure 7 (a) (at. %)

Point	U	Sb	Fe
1	62.4	37.3	0.3
2	63.9	34.4	1.7
3	60.0	38.9	1.1
4	60.5	38.5	1.0

For the U-4Sb/HT9 interface, there is a crack found between two alloys, it is probably due to the quenching. The sudden temperature drop could result in the change of sample shape, the crack could take place as the thermal expansion of U-4Sb alloy and HT9 are different. The crack, however, should not affect the chemical composition of the reaction layer. U is the matrix composition in U-4Sb alloy, Fe and Cr are the two major compositions in HT9. Per our analysis, the reactions between U-4Sb alloy and HT9 are taken place between those three elements. As marked in Figure 8 (a), the inter-diffusion layers are $U(Fe,Cr)_2$ at HT9 side and U_6Fe at U-4Sb alloy side. The diffusion pattern for U-4Sb/HT9 is analogous to U-4Sb/Fe, except for the composition in layer-II. To the best of our knowledge, there is no available data for U/HT9 diffusion couple tests, because when people started investigating HT9 as cladding for metallic fuel, they already consider U-10wt.%Zr as a driven fuel option [42]. However, the most relevant reference could be referred to U vs. Fe-15wt.%Cr [43] in which the author labeled the layer between U_6Fe and Fe-15wt.%Cr as UFe_2, but actually it does contain 12~20 at. % Cr. In this study, we denote this layer as $U(Fe,Cr)_2$. The results in this work, therefore, could provide an intuitive reference for the diffusion layers that could possibly formed between U and HT9. From Figure 8 (e), Cr is found to be enriched at the interface between HT9 and $U(Fe,Cr)_2$, this is resulted from faster diffusion of Fe into U (Cr was left behind) [43]. A line scan was performed in Figure 8 (a), and the data is shown in Figure 8 (f). According to the plot, layer-II or layer-III is found to be discontinued. It should be due to the vertical displacement of the fuel alloy and HT9 cladding at the interface. As mentioned above, a crack was formed due to the quenching. The fuel alloy and HT9 were separated, so they are not necessarily at the original place.

For U-Sb precipitates, they are similar to the Fe side. U-Sb precipitates are “kept” in U_6Fe, the point data indicates that Fe fraction in U-Sb precipitate is significantly drop to less than 1 at. % which could be treated as noise, therefore it is believed that Fe does not diffuse into those precipitates. Also, there is no Sb reactant found in HT9.

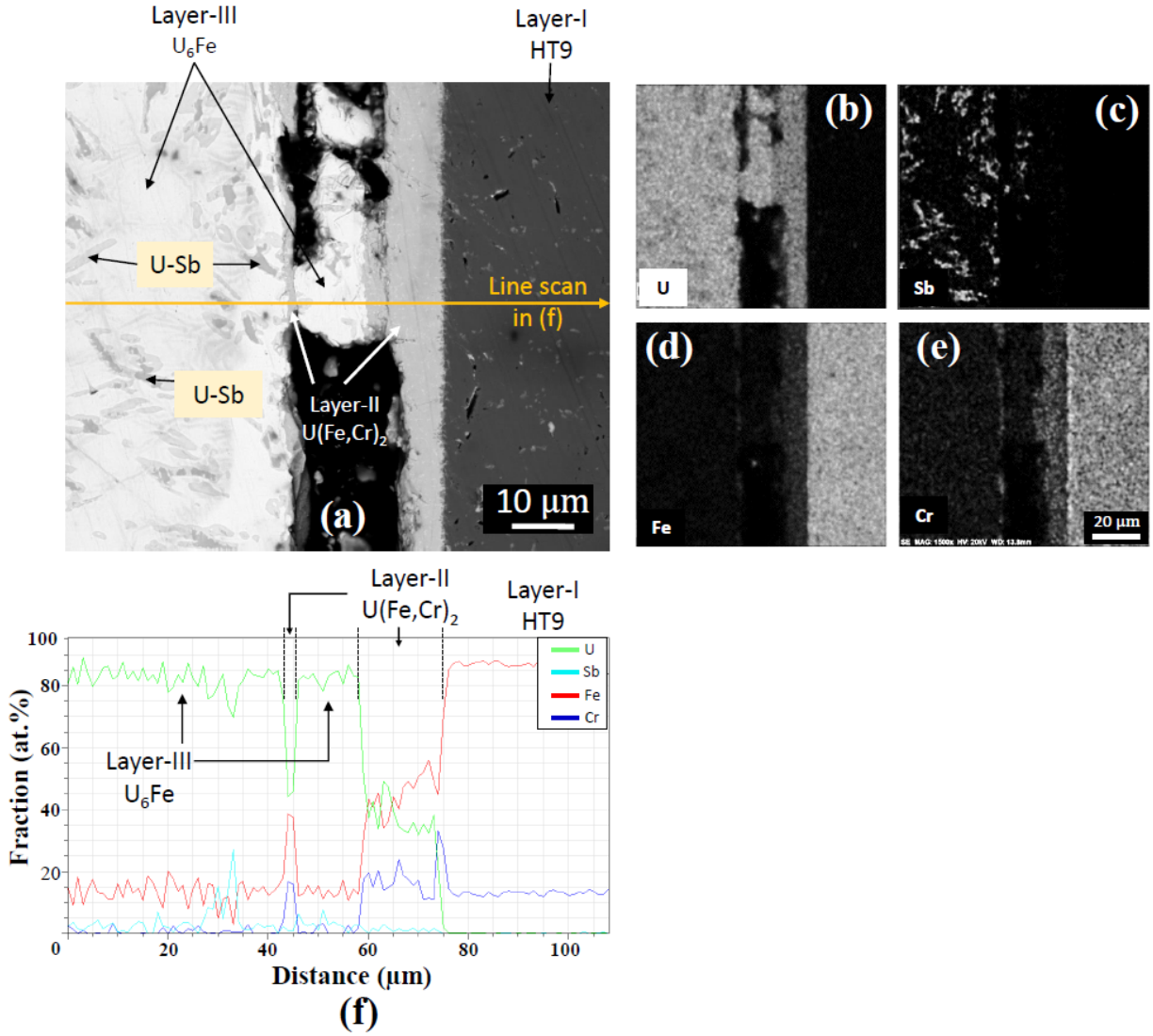

Figure 8. (a) U-4Sb/HT9 interface, (b)~(e) are elemental maps of U, Sb, Fe, and Cr for (a), (f) is the data of the line scan in (a).

3.2.2 U-4Sb-4Ce/cladding

Figure 9 (a) shows the BSE image of Fe/U-4Sb-4Ce, layer-II is UFe_2, layer-III contains U_6Fe (bright matrix), U-Sb and Ce-Sb precipitates. A round Ce-Sb precipitation circled out in Figure 9 (a) is zoomed in Figure 9 (b) at magnification of 25000×. The EDS point indicates the Ce-Sb precipitate being pointed at contains 33.7 % Ce, 36.0 % Sb, 28.5 % U, and 1.8 % Fe (atom percent). The ratio of Ce to Sb suggests that it could be CeSb phase, as mentioned in section 3.1.2. Since the Ce-Sb precipitate is around 1 µm (which is also equal to the EDS resolution), it is believed that the quantified point data are perturbed by the surrounding U_6Fe phase, resulting in the present of the U and Fe fraction. From the elemental map of Fe (Figure 9f), it is found that Fe is depleted in the CeSb phase. Further analysis is performed in U_6Fe layer, and the results are shown in Figure

10. The line scan is going across the U-Sb and Ce-Sb precipitates, and the Fe fraction drop close to zero when the line passes the Sb-precipitates, suggesting that Fe does not diffuse inside.

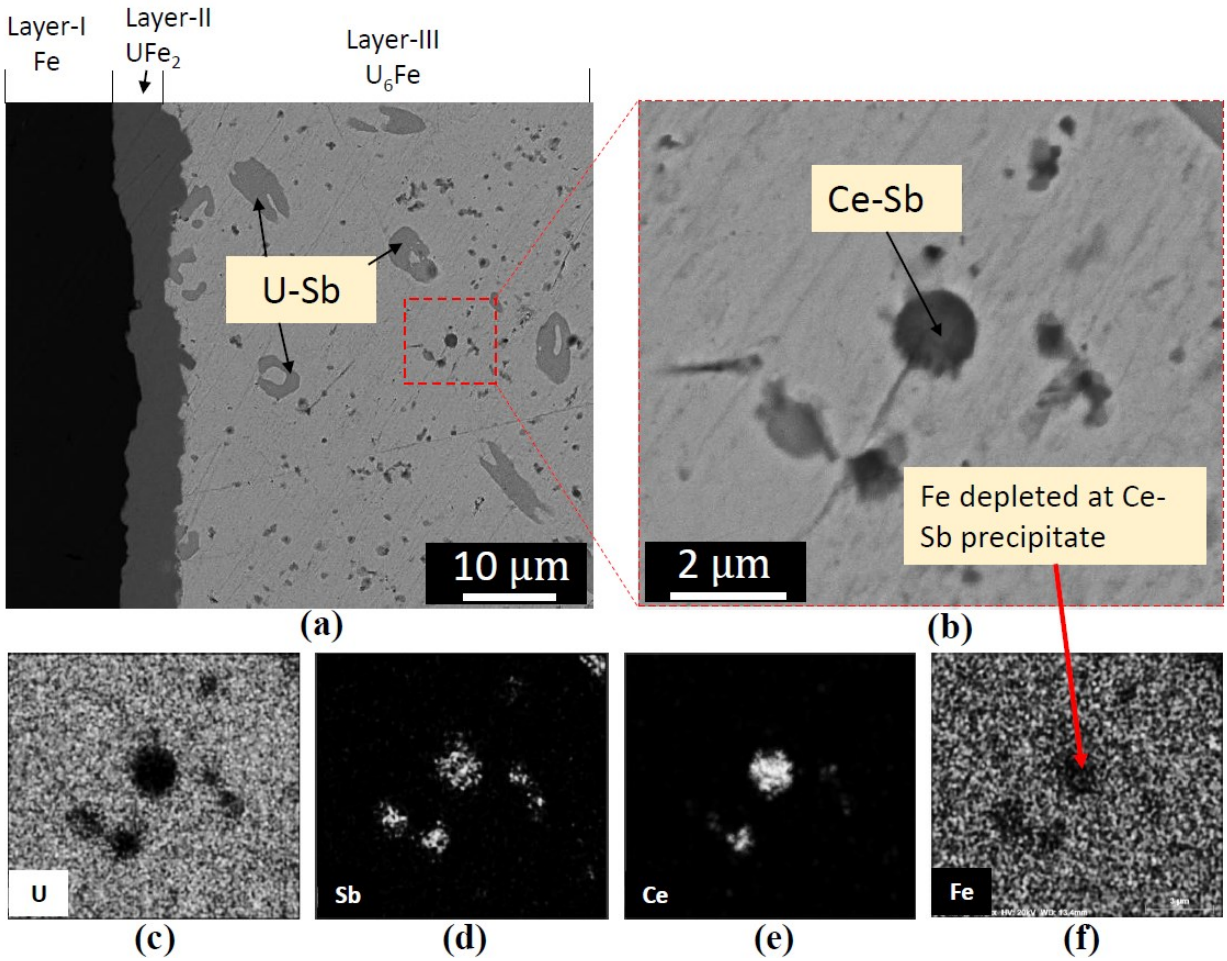

Figure 9. (a) U-4Sb-4Ce/Fe interface, (b) larger magnification of the area around Ce-Sb precipitation inside U_6Fe layer, (c)~(f) are elemental maps of U, Sb, Ce, and Fe for (b).

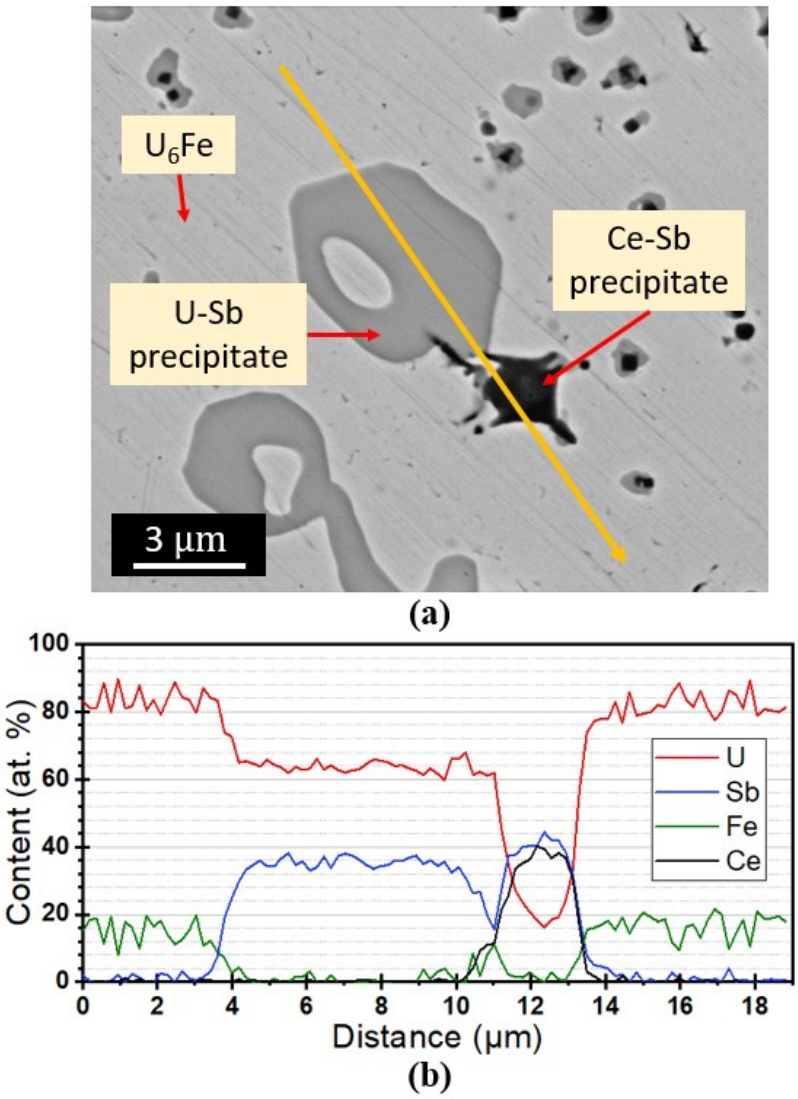

Figure 10. (a) BSE image showing Sb-precipitates inside the U_6Fe reaction layer from U-4Sb-4Ce/Fe interface, (b) elemental distribution corresponding to the scan line.

For HT9 side, because HT9 was separated from the coupled surface, two interfaces' cross sections are shown separately. One is U-4Sb-4Ce interface that was originally contacted with HT9 in Figure 11 (a), the other is HT9 interface that was originally contacted with U-4Sb-4Ce in Figure 11 (b). Layer-II are the laves phases $U(Fe,Cr)_2$ which is the same to the case presented in Figure 8. In layer-III the region contains Ce-Sb precipitates is enlarged in Figure 11 (c) and the corresponding maps are shown in Figure 11 (d) - (g). According to the Fe map, the Fe-depletion is found on those Ce-Sb precipitates, which is similar to that in Figure 9. Due to the limitation of the EDS spatial resolution, the point or line scan analysis on the Ce-Sb precipitates were not performed. Because this reaction layer is U_6Fe, the results could be analogues to that of U-4Sb-4Ce/Fe interface.

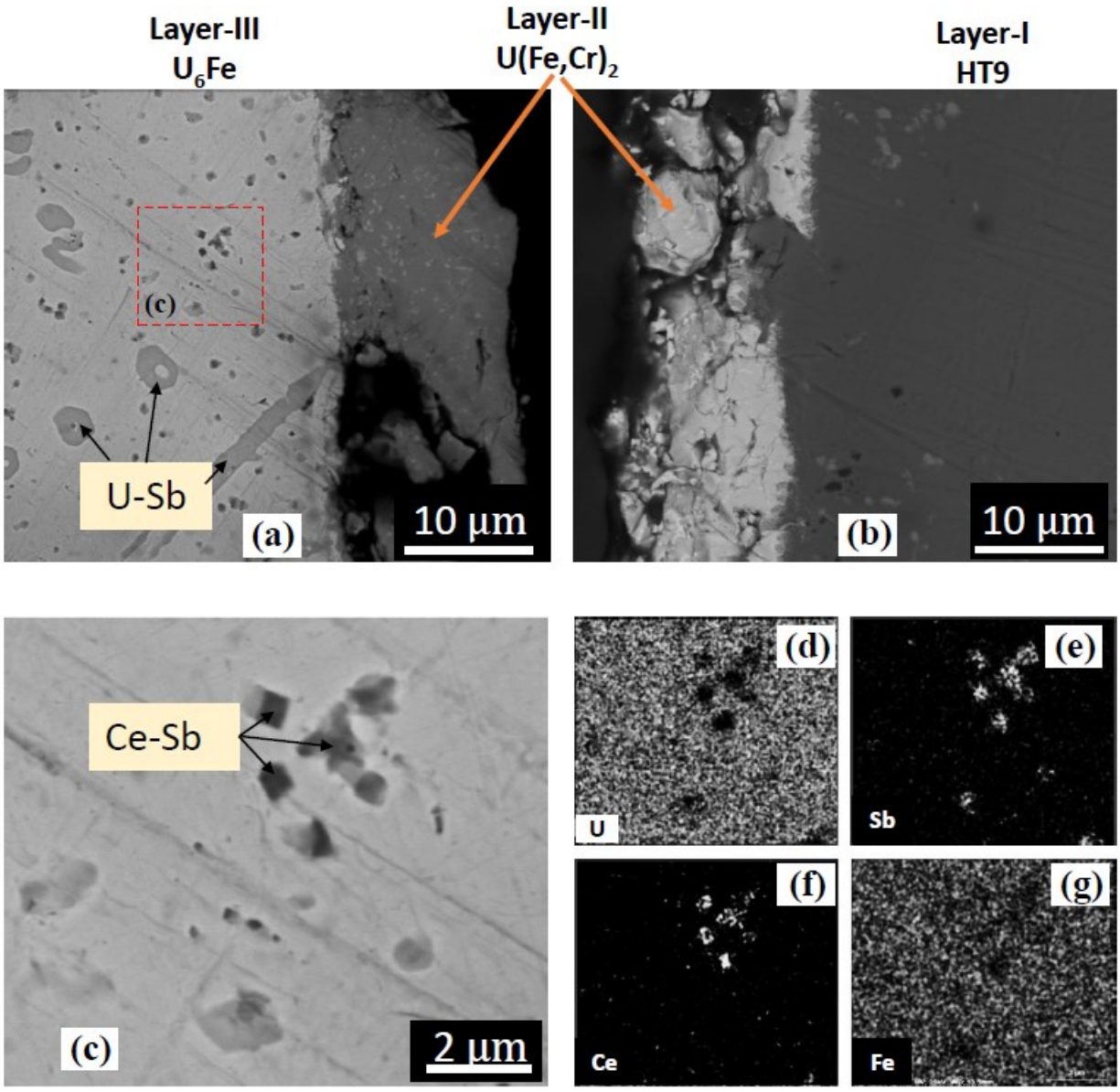

Figure 11. (a) U-4Sb-4Ce surface that was originally contacted with HT9, (b) HT9 surface that was originally contacted with U-4Sb-4Ce, (c) larger magnification of the area around Ce-Sb precipitation inside U_6Fe layer, (d)~(g) are elemental maps of U, Sb, Ce, and Fe for (c).

4. Conclusion

In the present study, U-4Sb and U-4Sb-4Ce alloys were analyzed using SEM/EDS. No free Sb metal was observed in both alloys. In U-4Sb alloys, Sb is in the form of precipitates with uranium. However, with Ce presented (i.e., U-4Sb-4Ce alloy), U-Sb precipitation decomposed, and Ce was bound by Sb to precipitate out. This suggests Sb could have higher affinity to Ce over U. Heat exposure tests do not change the morphologies of the precipitates.

Diffusion couple tests of U-4Sb/cladding and U-4Sb-4Ce/cladding were conducted and the interfaces were analyzed. The inter-diffusion behavior between USb alloys (U-4Sb or U-4Sb-4Ce) and cladding materials (Fe or HT9) suggests that the reaction layers are analogous to the U/Fe system. For U/ HT9 system the it is found that $U(Fe, Cr)_2$ is formed adjacent to HT9 and U_6Fe is formed adjacent to USb alloy. Reaction between Sb-precipitations and the cladding material (Fe or HT9) is not found. Sb-precipitations (U-Sb or Ce-Sb) are found in layer U_6Fe, they are stable, that they are not affected by the U-Fe reaction. By the diffusion behavior, it is suggested the laves phase (UFe_2 or $U(Fe,Cr)_2$) is formed by outward diffusion of uranium, while UFe_6 is formed by inward diffusion of Fe into the fuel alloy.

Sb is considered to be a promising additive for mitigating FCCI, this work is a supplementary material to illustrate the Sb function in pure U region of UZr fuel, it can also provide a pioneering view for Zr-free alloys as proposed in BN-type fast reactor. The in-pile tests are recommended in the future.

Acknowledgements

The authors acknowledge the Department of Nuclear Energy, Office of Nuclear Energy, Science, and technology, under DOE-NE Idaho Operations Office Contract DE-AC07-05ID14517 and the financial support of U.S. Department of Energy Nuclear Energy University Program, grant number DENE0008574. We thank Dr. Stuart A. Maloy of Los Alamos National Laboratory for kindly providing the HT9 sample. The advice and help by Nanoscale Characterization and Fabrication Laboratory at Virginia Tech is also highly appreciated.

References

[1] C. Matthews, C. Unal, J. Galloway, D.D. Keiser, S.L. Hayes, Fuel-cladding chemical interaction in U-Pu-Zr metallic fuels: A critical review, Nucl. Technol. 198 (2017) 231–259. doi:10.1080/00295450.2017.1323535.
[2] Y. Xie, J. Zhang, X. Li, J.P. Isler, M.T. Benson, R.D. Mariani, C. Unal, Lanthanide migration and immobilization in metallic fuels, Prog. Nucl. Energy. 109 (2018) 233–238. doi:10.1016/j.pnucene.2018.08.019.
[3] R.D. Mariani, D.L. Porter, T.P. O'Holleran, S.L. Hayes, J.R. Kennedy, Lanthanides in metallic nuclear fuels: Their behavior and methods for their control, J. Nucl. Mater. 419 (2011) 263–271. doi:10.1016/J.JNUCMAT.2011.08.036.
[4] J.M. Harp, L. Capriotti, F. Cappia, Baseline Postirradiation Examination of the AFC-3C , Experiments, 2018. doi:10.2172/1498255.
[5] M.T. Benson, J.A. King, R.D. Mariani, M.C. Marshall, SEM characterization of two advanced fuel alloys: U-10Zr-4.3Sn and U-10Zr-4.3Sn-4.7Ln, J. Nucl. Mater. 494 (2017) 334–341. doi:10.1016/j.jnucmat.2017.07.057.

[6] Y. Xie, M.T. Benson, J.A. King, R.D. Mariani, J. Zhang, Characterization of U-Zr fuel with alloying additive Sb for immobilizing fission product lanthanides, J. Nucl. Mater. 498 (2018) 332–340. doi:10.1016/j.jnucmat.2017.10.039.
[7] Y. Xie, J. Zhang, M.T. Benson, J.A. King, R.D. Mariani, Assessment of Te as a U-Zr fuel additive to mitigate fuel-cladding chemical interactions, J. Nucl. Mater. 513 (2019) 175–184. doi:10.1016/j.jnucmat.2018.10.050.
[8] Y.S. Kim, T. Wiencek, E. O'Hare, J. Fortner, A. Wright, J.S. Cheon, B.O. Lee, Effect of indium addition in U-Zr metallic fuel on lanthanide migration, J. Nucl. Mater. (2017). doi:10.1016/j.jnucmat.2016.11.012.
[9] G. Bozzolo, A.M. Yacout, G.L. Hofman, H.O. Mosca, Modeling of In, Tl, Ga, Sb, and Pd as lanthanides binding agents in U-Zr metallic nuclear fuels, in: Mater. Res. Soc. Symp. Proc, 2012: pp. 29–35. doi:10.1557/opl.2012.915.
[10] M.T. Benson, Y. Xie, J.A. King, K.R. Tolman, R.D. Mariani, I. Charit, J. Zhang, M.P. Short, S. Choudhury, R. Khanal, N. Jerred, Characterization of U-10Zr-2Sn-2Sb and U-10Zr-2Sn-2Sb-4Ln to assess Sn+Sb as a mixed additive system to bind lanthanides, J. Nucl. Mater. 510 (2018) 210–218. doi:10.1016/j.jnucmat.2018.08.017.
[11] M.T. Benson, Y. Xie, J.A. King, K.R. Tolman, R.D. Mariani, I. Charit, J. Zhang, M.P. Short, S. Choudhury, R. Khanal, N. Jerred, Characterization of U-10Zr-2Sn-2Sb and U-10Zr-2Sn-2Sb-4Ln to assess Sn+Sb as a mixed additive system to bind lanthanides, J. Nucl. Mater. 510 (2018) 210–218. doi:10.1016/j.jnucmat.2018.08.017.
[12] W. Zhuo, Y. Xie, M.T. Benson, Q. Yang, R.D. Mariani, J. Zhang, Experimental Investigation of FCCI using Diffusion Couple Test between UZr fuel with Sb additive and Cladding, Nucl. Sci. Eng. (2020). doi:10.1080/00295639.2020.1713656.
[13] Y. Xie, J. Zhang, M.T. Benson, R.D. Mariani, Thermodynamic stability studies of Ce-Sb compounds with Fe, J. Nucl. Mater. 499 (2018) 440–445. doi:10.1016/j.jnucmat.2017.12.008.
[14] Y. Xie, J. Zhang, M.T. Benson, R.D. Mariani, Diffusion behavior of lanthanide-additive compounds (Ce4Sb3, Ce2Sb, and CeTe) against HT9 and Fe, Mater. Charact. (2019). doi:10.1016/j.matchar.2019.02.012.
[15] G.L. Hofman, L.C. Walters, T.H. Bauer, Metallic fast reactor fuels, Prog. Nucl. Energy. 31 (1997) 83–110. doi:10.1016/0149-1970(96)00005-4.
[16] D.D. Keiser, Metal fuel-cladding interaction, in: Compr. Nucl. Mater., Elsevier, 2012: pp. 423–441. doi:10.1016/B978-0-08-056033-5.00067-7.
[17] J.M. Harp, D.L. Porter, B.D. Miller, T.L. Trowbridge, W.J. Carmack, Scanning electron microscopy examination of a Fast Flux Test Facility irradiated U-10Zr fuel cross section clad with HT-9, J. Nucl. Mater. 494 (2017) 227–239. doi:10.1016/J.JNUCMAT.2017.07.040.
[18] D. D. Keiser and M. A. Dayananda, Interdiffusion between U-Zr fuel and selected Fe-Ni-Cr alloys, J. Nucl. Mater., vol. 200, no. 2, pp. 229–243, Apr. 1993.
[19] G.W. Keilholtz, G.C. Battle, Fission product release and transport in liquid metal fast breeder reactors, Oak Ridge, Tennessee, 1969.
[20] A.L. Nichols, D.L. Aldama, M. Verpelli, Handbook of nuclear data for safeguards: database extentions, August 2008. International Atomic Energy Agency.
[21] T. Sakuma, K. Yamazaki, T. Nishizawa, A characteristic dislocation network resulting from the diffusion of antimony into iron single crystals, Scr. Metall. 10 (1976) 687–691.
[22] S.M. Myers, H.J. Rack, Ion-beam investigation of Sb diffusion and solubility in Fe, J. Appl. Phys. 49 (1978) 3246–3254. doi:10.1063/1.325272.

[23] H. Okamoto, Fe-Sb (Iron-Antimony), J. Phase Equilibria. 20 (1999) 166. doi:10.1007/s11669-999-0017-x.
[24] D.D. Keiser, M.A. Dayananda, Interdiffusion between U-Zr fuel vs selected cladding steels, Metall. Mater. Trans. A. 25 (1994) 1649–1653. doi:10.1007/BF02668530.
[25] C.T. Lee, H. Kim, T.K. Kim, C.B. Lee, Diffusion behavior in an interface between U – 10Zr alloy and HT-9 steel, J. Nucl. Mater. 395 (2009) 140–144. doi:10.1016/j.jnucmat.2009.10.044.
[26] Y.M. Golovchenko, Oxide-metal core is possible transition to the metal fuel core for fast reactors of the BN-Type, Int. J. Energy Power Eng. 2 (2013) 113. doi:10.11648/j.ijepe.20130203.15.
[27] Y.M. Golovchenko, Some results of developments and investigations of fuel pins with metal fuel for heterogeneous core of fast reactors of the BN-type, Energy Procedia. 7 (2011) 205–212. doi:10.1016/j.egypro.2011.06.027.
[28] P. Hosemann, S. Kabra, E. Stergar, M.J. Cappillo, S.A. Maloy, Micro-structural characterization of laboratory heats of the Ferric/Martensitic steels HT-9 and T91, J. Nucl. Mater. 403 (2010) 7–14. doi:10.1016/j.jnucmat.2010.05.005.
[29] J.J. Friel, C.E. Lyman, Microscopy microanalysis X-ray mapping in electron-beam instruments, Microsc. Microanal. 12 (2006) 2–25.
[30]https://web.archive.org/web/20190511222636/http://www.kayelaby.npl.co.uk/atomic_and_nuclear_physics/4_2/4_2_1.html
[31] B.J. Beaudry, A.H. Daane, The antimony-uranium alloy system, Trans. Met. Soc. AIME. 215 (1959).
[32] D.E. Newbury, N.W.M. Ritchie, Performing elemental microanalysis with high accuracy and high precision by scanning electron microscopy/silicon drift detector energy-dispersive X-ray spectrometry (SEM/SDD-EDS), J. Mater. Sci. 50 (2014) 493–518. doi:10.1007/s10853-014-8685-2.
[33] H. Okamoto, M.E. Schlesinger, E.M. Mueller, Sb (antimony) binary alloy phase diagrams, in: ASM handbook, Vol. 3 Alloy Phase Diagrams, 2016: pp. 585–590. doi:10.31399/asm.hb.v03.a0006202.
[34] J.A. Paixao, J. Rebizant, A. Blaise, A. Delapalme, J.P. Sanchez, G.H. Lander, H. Nakotte, P. Burlet, M. Bonnet, Magnetism of a new U-Sb phase: U5Sb4, Phys. B Condens. Matter. 203 (1994) 137–146.
[35] H. Okamoto, Ce-Sb (cerium-antimony), J. Phase Equilibria. 22 (2001) 88.
[36] W.S. Rasband, ImageJ, U. S. National Institutes of Health, Bethesda, Maryland, USA, https://imagej.nih.gov/ij/, 1997-2018.
[37] L. Paolasini, B. Hennion, Lattice dynamics of cubic Laves phase ferromagnets, Phys. Rev. B. 58 (1998) 125–133.
[38] A. Andreev, L. Havela, V. Sechovsky, The loss of magnetism in U(Fe, Cr)2, J. Phys. Colloq. 49 (1988) 49–51. doi:10.1051/jphyscol:19888219.
[39] E.C. Beahm, C.A. Culpepper, O.B. Cavin, Laves phases of uranium and 3d transition metals, J. Less-Common Met. 50 (1976) 57–71.
[40] K. Huang, Y. Park, A. Ewh, B.H. Sencer, J.R. Kennedy, K.R. Coffey, Y.H. Sohn, Interdiffusion and reaction between uranium and iron, J. Nucl. Mater. 424 (2012) 82–88. doi:10.1016/j.jnucmat.2012.02.004.
[41] T. Chen, T.A. Smith, J.G. Gigax, D. Chen, R. Balerio, L. Shao, B.H. Sencer, J.R. Kennedy, Intermetallic formation and interdiffusion in diffusion couples made of uranium and single crystal iron, J. Nucl. Mater. 467 (2015) 82–88. doi:10.1016/j.jnucmat.2015.05.026.

[42] R.G. Pahl, C.E. Lahm, S.L. Hayes, Performance of HT9 clad metallic fuel at high temperature, J. Nucl. Mater. 204 (1993) 141–147. doi:10.1016/0022-3115(93)90210-P.
[43] K. Huang, Diffusion and reaction in selected uranium alloy system, University of Central Florida, 2012.